



UNIVERSITI PUTRA MALAYSIA

**MICROSTRUCTURE, MAGNETIC AND ELECTRICAL PROPERTIES OF
 $\text{La}_{0.67}(\text{Sr}_{1-x}\text{Bax})_{0.33}\text{Mn}_{1-y}\text{TiyO}_3$**

ZALITA BINTI ZAINUDDIN

FS 2009 33



**MICROSTRUCTURE, MAGNETIC AND ELECTRICAL PROPERTIES OF
 $\text{La}_{0.67}(\text{Sr}_{1-x}\text{Ba}_x)_{0.33}\text{Mn}_{1-y}\text{Ti}_y\text{O}_3$**

By

ZALITA BINTI ZAINUDDIN

**Thesis Submitted to the School of Graduate Studies, Universiti Putra Malaysia,
in Fulfilment of the Requirement for the Degree of Doctor of Philosophy**

October 2009



DEDICATION

To my dearest husband, parents, sons, family and friends.



Abstract of thesis presented to the Senate of Universiti Putra Malaysia in fulfilment of the requirement for the degree of Doctor of Philosophy

**MICROSTRUCTURE, MAGNETIC AND ELECTRICAL PROPERTIES OF
 $\text{La}_{0.67}(\text{Sr}_{1-x}\text{Ba}_x)_{0.33} \text{Mn}_{1-y}\text{Ti}_y\text{O}_3$**

By

ZALITA BINTI ZAINUDDIN

October 2009

Chairman: Abdul Halim Shaari, PhD

Faculty: Science

A study on the microstructure, magnetic and electrical properties of $\text{La}_{0.67}\text{Sr}_{0.33}\text{MnO}_3$ substituted with Ba at Sr site and Ti at Mn site have been performed. Samples of $\text{La}_{0.67}(\text{Sr}_{1-x}\text{Ba}_x)_{0.33} \text{Mn}_{1-y}\text{Ti}_y\text{O}_3$ (LSBMT) with $x = 0.00, 0.25, 0.50, 0.75$ and 1.00 ; and $y = 0.00, 0.05, 0.10, 0.15, 0.20, 0.40$ and 0.60 were prepared using solid state reaction method. Quantitative compositional percentage data of the elements results confirmed the expected La:Sr:Ba:Mn:Ti ratios for the prepared samples. X-ray Diffractometer (XRD) spectrum showed single phase compounds, except for samples with $y = 0.60$ which have $\text{La}_2\text{Ti}_2\text{O}_7$ peaks. Sr substitution with Ba changed the rhombohedral $R\bar{3}c$ structure to cubic $Pm\bar{3}m$, however Mn substitution with Ti only increased the lattice parameters values, without changing the whole structure. Scanning Electron Microscope (SEM) images showed a few porous structured samples, with coarse and fine grains while the others showed large closely packed grains with clear shapes and grain boundaries. The magnetization studies showed that samples with $y = 0.00$ exhibited a transition from the ferromagnetic to the paramagnetic phase as temperature increased and the Curie temperature, T_C decreased from 371 K to 341 K when x increased from 0.00 to 1.00. T_C also

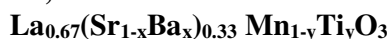


decreased when y increased. Magnetization versus field patterns did not differ much with x composition. The ferromagnetic behaviour for $0.00 \leq y \leq 0.15$ change to paramagnetic when $y \geq 0.20$. Resistivity versus temperature study showed that samples with $y = 0.00$ had metal-like behaviour. Nearly all samples with $0.00 < y < 0.20$ showed metallic and semiconducting-like behaviour. LSBMT with $y \geq 0.20$ exhibited only semiconducting behaviour. The metal-insulator transition temperature, T_p decreased with increment of x and/or y . At $T < T_p$ the resistivity curves can be fitted with the $\rho = \rho_0 + \rho_2 T^2$ relations. For $T > T_p$ the curves can be fitted with the variable range hopping (VRH) model and small polaron hopping (SPH) model. The density of states at Fermi level, $N(E_F)$ values were between 10^{18} to 10^{22} eV⁻¹cm⁻³. Polaron activation energy, E_p increased with y ranging from 47 meV to 210 meV. Magnetoresistance (MR) measurement showed an increment of the MR % when the magnetic field increased and temperature decreased. The maximum MR % was ~34 % for LSBMT with $x = 0.00$ and $y = 0.15$ at 100 K and 1.0 Tesla. Samples with $y \leq 0.10$ showed low field magnetoresistance (LFMR) effect. At 1000 Hz LSBMT with $x = 0.00, 0.25$ and 0.75 exhibit a ferroelectric-paraelectric transition peak at 200 K, 250 K and 225 K respectively, with the highest ϵ' value of 6.54×10^5 when $x = 0.25, y = 0.20$. The Nyquist plots of Z'' versus Z' showed depressed semicircles contributed by the grain, grain boundary and/or electrode effect. Two relaxation processes occurred in the AC conductivity curve due to the grain and grain boundary. Materials with very high dielectric constant $\sim 10^5$ at 1000 kHz were successfully synthesized with $x \leq 0.75; y = 0.20$ and all samples with $y = 0.40$. Samples with $y = 0.40$ have wide range of nearly frequency and temperature independent high dielectric constant. These samples are excellent for capacitors fabrication.



Abstrak tesis yang dikemukakan kepada Senat Universiti Putra Malaysia
sebagai memenuhi keperluan untuk ijazah Doktor Falsafah

MIKROSTRUKTUR, SIFAT MAGNET DAN SIFAT ELEKTRIK



Oleh

ZALITA BINTI ZAINUDDIN

Oktober 2009

Pengerusi: Abdul Halim Shaari, PhD

Fakulti: Sains

Kajian ke atas mikrostruktur, sifat magnet dan sifat elektrik $\text{La}_{0.67}\text{Sr}_{0.33}\text{MnO}_3$ yang diganti dengan Ba di tempat Sr dan Ti di tempat Mn telah dilakukan. Sampel-sampel $\text{La}_{0.67}(\text{Sr}_{1-x}\text{Ba}_x)_{0.33} \text{Mn}_{1-y}\text{Ti}_y\text{O}_3$ (LSBMT) dengan $x = 0.00, 0.25, 0.50, 0.75$ dan 1.00 ; dan $y = 0.00, 0.05, 0.10, 0.15, 0.20, 0.40$ dan 0.60 telah disediakan mengguna kaedah tindak balas keadaan pepejal. Data peratusan komposisi kuantitatif bagi unsur mengesahkan nisbah La:Sr:Ba:Mn:Ti jangkaan bagi sampel yang disediakan. Spektrum Pembelauan Sinar-X (XRD) menunjukkan sebatian berfasa tunggal, kecuali bagi sampel dengan $y = 0.60$ yang mempunyai puncak-puncak $\text{La}_2\text{Ti}_2\text{O}_7$. Penggantian Sr dengan Ba mengubah struktur rhombohedral $R\bar{3}c$ kepada kubik $Pm\bar{3}m$, tetapi penggantian Mn dengan Ti hanya meningkatkan nilai pemalar kekisi, tanpa mengubah struktur keseluruhan. Imej Mikroskop Elektron Imbasan (SEM) menunjukkan beberapa sampel berstruktur porous, dengan butiran yang kasar dan halus manakala yang lainnya menunjukkan butiran besar yang tersusun padat dengan bentuk dan sempadan butiran yang jelas. Kajian pemagnetan menunjukkan bahawa sampel dengan $y = 0.00$ mempamerkan peralihan daripada fasa feromagnet kepada paramagnet apabila suhu ditingkatkan dan suhu Curie, T_C berkurang dari 371 K



kepada 341 K apabila x meningkat dari 0.00 kepada 1.00. T_C turut berkurang apabila y meningkat. Corak pemagnetan tidak banyak berubah dengan komposisi x . Sifat feromagnet bagi $0.00 \leq y \leq 0.15$ berubah kepada paramagnet bagi $y \geq 0.20$. Kajian kerintangan melawan suhu menunjukkan bahawa sampel dengan $y = 0.00$ mempunyai kelakuan seperti logam. Hampir kesemua sampel dengan $0.00 < y < 0.20$ menunjukkan kelakuan seperti logam dan semikonduktor. LSBMT dengan $y \geq 0.20$ hanya menunjukkan kelakuan semikonduktor. Suhu peralihan logam-penebat, T_P berkurang dengan penambahan x dan/atau y . Pada $T < T_P$ lengkung kerintangan boleh dipadankan dengan hubungan $\rho = \rho_0 + \rho_2 T^2$. Bagi $T > T_P$ lengkung boleh dipadankan dengan model Loncatan Julat Boleh ubah (VRH) dan model Loncatan Polaron Kecil (SPH). Nilai ketumpatan keadaan di aras Fermi adalah di antara 10^{18} to $10^{22} \text{ eV}^{-1} \text{ cm}^{-3}$. Tenaga pengaktifan polaron, E_p meningkat dengan y dalam julat 47 meV kepada 210 meV. Pengukuran magnetorintangan menunjukkan peningkatan MR % apabila medan magnet meningkat dan suhu berkurang. MR % maksimum adalah ~34 % bagi LSBMT dengan $x = 0.00$ dan $y = 0.15$ pada 100 K dan 1.0 Tesla. Sampel dengan $y \geq 0.10$ menunjukkan kesan magnetorintangan medan rendah (LFMR). Pada 1000 Hz sampel dengan $x = 0.00, 0.25$ and 0.75 menunjukkan puncak peralihan feroelektrik-paraelektrik pada 200 K, 250 K dan 225 K masing-masing, dengan nilai ϵ' tertinggi iaitu 6.54×10^5 apabila $x = 0.25, y = 0.20$. Plot Nyquist bagi Z'' melawan Z' menunjukkan separa bulatan terhimpit yang disumbangkan oleh butiran, sempadan butiran dan/atau elektrod. Dua proses perelatan berlaku pada lengkung kekonduksian AC disebabkan oleh sempadan butiran pada frekuensi rendah dan butiran pada suhu tinggi. Bahan dengan pemalar dielektrik sangat tinggi $\sim 10^5$ pada 1000 kHz telah berjaya dihasilkan dengan sampel $x \leq 0.75; y = 0.20$ dan semua sampel dengan $y = 0.40$. Sampel dengan $y = 0.40$ mempunyai pemalar dielektrik



tinggi yang hampir tidak bergantung pada suhu dan frekuensi dalam suatu julat yang lebar. Sampel-sampel ini sangat sesuai untuk pembuatan kapasitor.



ACKNOWLEDGEMENTS

I would like to express my heart-felt gratitude to my supervisor, Professor Dr. Abdul Halim Shaari, for his wise guidance, advice and encouragement throughout this project. I would also like extend my appreciation to my co-supervisors Prof. Madya Dr Zainal Abidin Talib, Prof. Madya Dr. Hishamuddin Zainuddin and Dr. Lim Kean Pah for their support and suggestions. The financial support and study leave from the Ministry of Higher Education and Universiti Kebangsaan Malaysia is gratefully acknowledged. Many thanks also go to my friends for their friendships and generous help throughout my few years in UPM. Last but not least, I would like to give my deepest appreciation to my husband, parents and family members for their love and continuous support, encouragement and patience. I would have achieved nothing without them. Irsyad and Mirza, you are my inspiration.



I certify that an examination committee has met on 12 October 2009 to conduct the final examination of Zalita binti Zainuddin on her doctor Doctor of Philosophy thesis entitled “Microstructure, Magnetic And Electrical Properties Of $\text{La}_{0.67}(\text{Sr}_{1-x}\text{Ba}_x)_{0.33}\text{Mn}_{1-y}\text{Ti}_y\text{O}_3$ ” in accordance with Universiti Pertanian Malaysia (Higher Degree) Regulations 1981. The Committee recommends that the candidate be awarded the relevant degree. Members of the Examination Committee are as follows:

Kaida Khalid, PhD

Professor/Associate Professor
Faculty of Science
Universiti Putra Malaysia
(Chairman)

Elias Saion, PhD

Professor Associate/Professor
Faculty of Science
Universiti Putra Malaysia
(Internal Examiner)

W Mohamad Daud W Yusoff, PhD

Professor Associate/Professor
Faculty of Science
Universiti Putra Malaysia
(Internal Examiner)

Ibrahim Abu Talib, PhD

Professor
Faculty of Science and Technology
Universiti Kebangsaan Malaysia
(External Examiner)

BUJANG KIM HUAT, PhD

Professor and Deputy Dean
School of Graduate Studies
Universiti Putra Malaysia

Date:



This thesis submitted to the Senate of Universiti Putra Malaysia and has been accepted as fulfilment of the requirement for the degree of Doctor of Philosophy. The members of the Supervisory Committee were as follows:

Abdul Halim Shaari, PhD

Professor
Faculty of Science
Universiti Putra Malaysia
(Chairman)

Zainal Abidin Talib, PhD

Associate Professor
Faculty of Science
Universiti Putra Malaysia
(Member)

Hishamuddin Zainuddin, PhD

Associate Professor
Faculty of Science
Universiti Putra Malaysia
(Member)

Lim Kean Pah, PhD

Faculty of Science
Universiti Putra Malaysia
(Member)

HASANAH MOHD. GHAZALI, PhD

Professor and Dean
School of Graduate Studies
Universiti Putra Malaysia

Date: 14 January 2010



DECLARATION

I hereby declare that the thesis is based on my original work except for quotations and citations which have been duly acknowledged. I also declare that it has not been previously or concurrently submitted for any other degree at UPM or other institutions.

ZALITA BINTI ZAINUDDIN

Date: 4 February 2010



TABLE OF CONTENTS

	Page
DEDICATION	ii
ABSTRACT	iii
ABSTRAK	v
ACKNOWLEDGEMENTS	viii
APPROVAL	ix
DECLARATION	xi
LIST OF TABLES	xiv
LIST OF FIGURES	xv
LIST OF ABBREVIATIONS	xx
CHAPTER	
1 INTRODUCTION	1
2 LITERATURE REVIEW	6
2.1 Introduction	6
2.2 Perovskite manganite	7
2.3 $\text{La}_{1-x}\text{Sr}_x\text{MnO}_3$	8
2.4 Doped $\text{La}_{0.67}\text{Sr}_{0.33}\text{MnO}_3$	11
2.4.1 Substitution at La site	12
2.4.2 Substitution at Sr site	13
2.4.3 Substitution at Mn site	14
2.5 $\text{La}_{1-x}\text{Ba}_x\text{MnO}_3$ and Doped $\text{La}_{0.67}\text{Ba}_{0.33}\text{MnO}_3$	15
2.6 Dielectric studies on manganites	18
3 THEORY	
3.1 LaMnO_3	20
3.2 Jahn-Teller effect	21
3.3 Mixed valence lanthanum manganites	22
3.4 Some basic properties of the lanthanum manganites	25
3.4.1 Exchange mechanisms	25
3.4.2 Jahn-Teller Polaron	27
3.4.3 Ferromagnetic-Paramagnetic Transition	28
3.4.4 Transport Properties	28
3.4.5 Intrinsic and extrinsic CMR	30
3.5 Polarization and relative permittivity	34
3.6 Impedance spectroscopy	36
3.6.1 Universal capacitors	38
3.6.2 AC conductivity	39
4 METHODOLOGY	42
4.1 Samples Preparation	42
4.2 Samples Characterization	45
4.2.1 Phase and crystal structure determination	45
4.2.2 Microstructure and composition	46
4.2.3 Magnetic measurement	46
4.2.4 Resistance-Temperature characteristic	47



4.2.5	Magnetoresistance	49
4.2.6	Dielectric permittivity, impedance spectroscopy and AC conductivity	50
5	RESULTS AND DISCUSSION	
5.1	Composition analysis	52
5.2	Phase, structure and lattice parameters	56
5.3	Microstructure	66
5.4	Magnetization studies	75
5.4.1	Magnetization versus temperature	75
5.4.2	Magnetization versus field	82
5.5	Resistivity versus temperature	90
5.5.1	Low temperature conduction ($T < T_p$)	98
5.5.2	High temperature conduction ($T > T_p$)	102
5.6	Magnetoresistance properties	114
5.7	Dielectric study	125
5.7.1	Variation of dielectric properties with frequency	125
5.7.2	Variation of dielectric properties with temperature	136
5.7.3	Variation of dielectric properties with Ba and Ti content	143
5.8	Impedance spectroscopy analysis	152
5.8.1	Nyquist plots of Z'' versus Z'	152
5.8.2	Impedance variation with frequency	170
5.8.3	AC conductivity	178
6	CONCLUSIONS AND SUGGESTIONS	184
	REFERENCES	188
	BIODATA OF STUDENT	196
	LIST OF PUBLICATIONS	196



LIST OF TABLES

Table		Page
4.1.1	List of chemicals.	39
5.1.1	La, Sr, Ba, Mn and Ti atomic % with different x and y composition.	55
5.2.1	The structure, space group, lattice parameters (<i>a</i> and <i>c</i>), unit cell volume (<i>V</i>) and mean square deviation of LSBMT with different x and y = 0.00.	59
5.5.1	The best fit parameters of ρ_{01} , ρ_2 , R^2_1 , ρ_0 , $\rho_{2.5}$ and R^2_2 obtained from fitting experimental resistivity ($T < T_p$) with equation (3.3) and (3.4) for LSBMT with different x and (a) y = 0.00 and (b) y = 0.05.	100
5.5.2	T_p and parameters obtained from the best fitting of the resistivity data with the VRH models for LSBMT with different x and y = 0.05, 0.10 and 0.15.	108
5.5.3	Parameters obtained from the best fitting of the resistivity data with the VRH model for LSBMT with different x and y = 0.20 and 0.40.	110
5.5.4	The E_p and R^2 value for LSBMT with x = 0.05 and 0.10 fitted with the SPH model.	111
5.5.5	The E_p and R^2 value for LSBMT with x = 0.20 and 0.40 fitted with the SPH model.	113
5.5.6	The E_a and R^2 values of LSBMT with y = 0.60.	113
5.8.1	Value of R_b , C_b , R_{gb} , C_{gb} , R_e and C_e for the selected LSBMT.	165



LIST OF FIGURES

Figure		Page
2.1.1	ABO ₃ perovskite crystal structure	7
2.3.1	Resistivity vs. temperature for various La _{1-x} Sr _x MnO ₃ . Arrows indicate T_C as determined by magnetization measurement and the open triangles indicate anomalies due to structural transition (Urushibara et al., 1995).	8
2.3.2	The (a) magnetic, electronic and (b) structural phase diagrams of La _{1-x} Sr _x MnO ₃ . PI, PM, CI, FI, FM, and AFM denote the paramagnetic insulating, paramagnetic metallic, spin-canted insulating, ferromagnetic insulating, ferromagnetic metallic, and antiferromagnetic (A-type) metallic (AFM) states, respectively. T_C is the Curie temperature and T_N is the Neel temperature (Tokura and Tomioka, 1999; Asamitsu et al., 1996).	9
2.3.3	The (x, T) phase diagram of La _{1-x} Sr _x MnO ₃ . The structural (O, O', O'', R), magnetic (PM, CA, FM), and electronic (M, I) phases are indicated. Open symbols (dashed lines) denote structural phase boundaries; solid symbols (full lines) denote magnetic phase boundaries (Paraskevopoulos et al., 2000).	10
3.1.1	(a) The structure of ideal LaMnO ₃ perovskite and (b) one of the spins arrangements of an A-type magnetic ordering.	20
3.2.1	Crystal-field splitting of the five-fold degenerate atomic 3d levels into lower t_{2g} and higher e_g levels. JT distortion further lifts each degeneracy (Tokura & Tomioka, 1999).	22
3.3.1	Q_1 , Q_2 and Q_3 are the distortion modes of the MnO ₆ octahedron in the manganites system.	24
3.3.2	Structures of distorted perovskite of manganites: (a) orthorhombic and (b) rhombohedral (Tokura & Tomioka, 1999).	24
3.4.1	Schematic view of the DE mechanism (Haghiri-Gosnet & Renard, 2003).	26
3.4.2	Temperature dependence of resistivity for a La _{1-x} Sr _x MnO ₃ ($x = 0.175$) crystal at various magnetic fields. Open circles represent the magnitude of negative magnetoresistance with a magnetic field of 15 T (Tokura & Tomioka, 1999).	29
3.5.1	An example of real impedance, Z' versus imaginary impedance, Z'' plot with three arcs.	34
4.1.1	The overall experimental procedure.	43
4.1.2	Schematic representation of (a) calcining and (b) sintering process for preparation of manganite ceramics.	45
4.2.1	Schematic configuration of the four point probe	48
4.2.2	Schematic configuration of the four point probe.	43
5.1.1	The EDX spectrum for selected samples of LSBMT with the La:Sr:Ba:Mn:Ti atomic % ratio.	53, 54
5.2.1	XRD patterns (a) of LSBMT with different x and y = 0.00; and (b) the most intense peak.	57
5.2.2	(a)-(e): XRD patterns of LSBMT with different x and y = 0.05, 0.10, 0.15, 0.20, 0.40 and 0.60 (* is the La ₂ Ti ₂ O ₇ peak).	61-62



5.2.3	XRD patterns of LSBMT with different y composition; with (a) x = 0.00 and (b) x = 1.00 (* is the La ₂ Ti ₂ O ₇ peak).	63
5.2.4	Lattice parameter, a and c versus Ti composition, y for LSBMT with (a) x = 0.00 and (b) x = 1.00.	65
5.2.5	Unit cell volume, V versus Ti composition, y for LSBMT with different Ba, x composition.	66
5.3.1	(a)–(e): SEM images of LSBMT with different x and y = 0.00 with the estimated grain size value. The circle in each picture shows formation of grain boundary.	68
5.3.2	(a)–(e): SEM images of LSBMT with different x and y = 0.05 with the estimated grain size value.	69
5.3.3	(a)–(d): SEM images of LSBMT with different x and y = 0.20 with the estimated grain size value. The multi-step growth and the octagonal shaped tip are shown in (b).	70
5.3.4	(a)–(j): SEM images of LSBMT with different x and y = 0.40 with magnification of 1000 times (left) and 7000 times (right).	71-72
5.3.5	(a)–(e): SEM images of LSBMT with different x and y = 0.06 with the estimated grain size value.	74
5.3.6	Average grain size variation with x for LSBMT with different y. The dotted lines are as guide for the eyes.	75
5.4.1	Magnetization versus temperature (<i>M-T</i>) curves for samples with different x and y = 0.00 in applied magnetic field of 1000 Oe.	77
5.4.2	Derivation of magnetization with temperature, dM/dT and magnetization versus temperature curve for sample with x = 0.50, y = 0.00 in applied magnetic field of 1000 Oe.	77
5.4.3	Variation of Curie temperature (<i>T_C</i>) with x for samples with y = 0.00; with their <i>T_C</i> values.	78
5.4.4	<i>M-T</i> curves for LSBMT with different x and y = 0.05 in magnetic field of 1000 Oe.	79
5.4.5	<i>M-T</i> curves for LSBMT with x = 0.00, and different y; in an applied magnetic field of 1000 Oe.	80
5.4.6	<i>M-T</i> curves for LSBMT with (a) x = 0.50 and (b) x = 1.00; and y = 0.00 and 0.05 in an applied magnetic field of 1000 Oe	81
5.4.7	Magnetization versus applied magnetic field (<i>M-H</i>) curves of LSBMT with different x and y = 0.00.	83
5.4.8	Enlargement of the <i>M-H</i> curve for LSBMT with (a) x = 0.00 and (b) x = 1.00; and y = 0.00 around zero field.	84
5.4.9	<i>M-H</i> curves of LSBMT with different x and (a) y = 0.05 and (b) y = 0.20.	85
5.4.10	<i>M-H</i> curves of LSBMT with x = 0.25 and different y of (a) 0.00 to 0.10 and (b) 0.15 to 0.60.	87
5.4.11	<i>M-H</i> curves of LSBMT with x = 0.75 and different y of (a) 0.00 to 0.10 and (b) 0.15 to 0.60.	88
5.4.12	Variation of magnetization, <i>M</i> with x at 10 kOe for LSBMT with different y composition.	89
5.5.1	Temperature variation of the electrical resistivity (<i>ρ-T</i>) for LSBMT with different x and y = 0.00.	90
5.5.2	<i>ρ-T</i> curves of LSBMT with different x and (a) y = 0.05 and (b) y = 0.10. <i>T_p</i> is marked with the darkened symbols.	92



5.5.3	The ρ - T graph for LSBMT with different x and y = 0.15.	93
5.5.4	The ρ - T graph for LSBMT with different x and y = 0.20.	94
5.5.5	Metal-insulator transition temperature, T_p versus x for LSBMT with y = 0.05, 0.10 and 0.15.	95
5.5.6	The ρ - T graph for LSBMT with (a) x = 0.00 and (b) x = 1.00; and different y.	96
5.5.7	The best fit curves at lower temperature using equation (3.3) (straight lines) and (3.4) (dotted lines) for LSBMT with different x and; y = 0.00 and (b) y = 0.05.	99
5.5.8	(a) ρ_{01} , (b) ρ_2 and resistivity at T_p , ρ_{T_p} (symbols in black) variation with x for LSBMT at different y concentration.	101-102
5.5.9	Ln ρ versus $1000/T$ above T_p (indicated by the arrow) for samples with different x and y = 0.05. The solid lines are the best fit to equation (3.8).	103
5.5.10	Ln ρ versus $1000/T$ for LSBMT with different x and y = 0.20. The solid lines are the best fit to equation (3.8).	104
5.5.11	Ln ρ versus $1000/T$ for LSBMT with different x and (a) y = 0.40 and (b) y = 0.60. The solid lines are the best fit to equation (3.8).	105-106
5.5.12	Ln ρ versus $T^{-1/4}$ plot for LSBMT with different x and y = 0.05. The solid lines indicate the best fit to the VRH model.	107
5.5.13	Ln ρ versus $T^{-1/4}$ plot for LSBMT with different x and y = 0.40. The solid lines indicate the best fit to the VRH model.	109
5.5.14	Variation of $\ln(\rho/T)$ as a function of inverse temperature ($1000/T$) above T_p for LSBMT with different x and y = 0.05. The solid line gives the best fit to the SPH model.	111
5.5.15	Variation of $\ln(\rho/T)$ as a function of inverse temperature ($1000/T$) above T_p for LSBMT with different x and y = 0.20. The solid line gives the best fit to the SPH model.	112
5.6.1	(a)-(d) MR % versus applied field for LSBMT with x = 0.50 and y = 0.00, 0.05, 0.10 and 0.15. Dotted line separates the LFMR and HFMR.	116-117
5.6.2	(a)-(c) MR % as a function of the applied field (H) for LSBMT with x = 0.50 with different y concentrations at 100 K, 200 K and 300 K.	119
5.6.3	MR % as a function of x with different y, with applied magnetic field of 1.0 T and 0.1 T at temperature of (a) 100 K and (d) 300 K.	122
5.6.4	MR % versus temperature with applied field of 1.0 T and 0.1 T for LSBMT with different x and (a) y = 0.05 and (b) y = 0.15.	124
5.7.1	The (a) dielectric constant, ϵ' and (b) dielectric loss, ϵ'' variation with frequency, f at different temperature for LSBMT with (a) x = 0.00, y = 0.00 and (b) x = 1.00, y = 0.00. Dotted line represents the slope, m = -1.	126
5.7.2	The (a) ϵ' , (b) ϵ'' and (c) $\tan \delta$ variation with frequency at different temperature for LSBMT with x = 0.00, y = 0.20.	129
5.7.3	The (a) ϵ' , (b) ϵ'' and (c) $\tan \delta$ variation with frequency at different temperature for LSBMT with x = 1.00, y = 0.20.	131



5.7.4	The (a) ϵ' , (b) ϵ'' and (c) $\tan \delta$ variation with frequency at different temperature for LSBMT with $x = 0.50$, $y = 0.40$.	133
5.7.5	The (a) ϵ' , (b) ϵ'' and (c) $\tan \delta$ variation with frequency at different temperature for LSBMT with $x = 1.00$, $y = 0.60$.	135
5.7.6	The (a) ϵ' and (b) $\log \tan \delta$ variation with temperature at different frequency for LSBMT with $x = 0.00$, $y = 0.20$.	137
5.7.7	The (a) ϵ' and (b) $\log \tan \delta$ variation with temperature at different frequency for LSBMT with $x = 1.00$, $y = 0.20$.	139
5.7.8	The (a) ϵ' and (b) $\tan \delta$ variation with temperature at different frequency for LSBMT with $x = 0.50$, $y = 0.40$.	141
5.7.9	The (a) ϵ' and (b) $\tan \delta$ variation with temperature at different frequency for LSBMT with $x = 1.00$, $y = 0.60$	142-143
5.7.10	ϵ' variation with temperature for LSBMT with different x and $y = 0.20$ at (a) 10 Hz, (b) 1000 Hz and (c) 100000 Hz.	144
5.7.11	$\tan \delta$ variation with temperature for LSBMT with different x and $y = 0.20$ at (a) 10 Hz, (b) 1000 Hz and (c) 100000 Hz.	146
5.7.12	ϵ' and $\tan \delta$ variation with temperature for LSBMT with different x and (a) $y = 0.40$ and (b) $y = 0.60$ at 1000 Hz.	148
5.7.13	ϵ' and $\tan \delta$ variation with temperature for LSBMT with different y and $x =$ (a) 0.00, (b) 0.25, (c) 0.50, (d) 0.75 and (e) 1.00 at 1000 Hz.	149-151
5.8.1	Complex impedance spectrum of LSBMT with $x = 0.00$, $y = 0.20$ at different temperature with the equivalent circuit (inset of (a) and (b)). The solid lines represent the best fitting data and the darkened spots in (a) show the frequency at that point.	155-156
5.8.2	Complex impedance plot of LSBMT with $x = 1.00$, $y = 0.20$ at different temperature. (a)(ii) is the enlargement of the rectangle in (a)(i). The solid lines represent the best fitting data.	158-159
5.8.3	Complex impedance plot of LBMT0 with $x = 0.50$, $y = 0.40$ at different temperature with the equivalent circuit (inset (a)). The solid lines represent the best fitting data.	160-161
5.8.4	Complex impedance plot of LSBMT with $x = 0.50$, $y = 0.60$ at different temperature with the equivalent circuit (inset (c)). The solid lines represent the best fitting data.	163-164
5.8.5	Bulk and grain boundary resistivity variation with temperature of LSBMT with different x and $y = 0.20$, 0.40 and 0.60. The solid line is the guidance for the eyes.	166-167
5.8.6	Bulk resistivity and grain boundary resistivity variation with $1000/T$ for the selected LSBMT samples. The solid line is the best slope.	168
5.8.7	The bulk and grain boundary activation energy variation with x and y for the LSBMT samples.	169
5.8.8	Variation of real part of impedance, Z' as a function of frequency at different temperatures for the selected LSBMT samples.	171-173
5.8.9	Variation of imaginary part of impedance, Z'' as a function of frequency for the selected LSBMT samples at different temperatures.	176-177
5.8.10	Variation of σ_{ac} with frequency for LSBMT sample with $x = 0.00$, $y = 0.20$. I, II and III in denotes different regions.	179



5.8.11	Variation of σ_{ac} with f at different temperatures for LSBMT sample with $x = 1.00$ and $y = 0.20$. I and II denotes different regions.	180
5.8.12	Variation of σ_{ac} with f at different temperatures for samples with (a) $x = 0.50$, $y = 0.40$ and (b) $x = 1.00$, $y = 0.60$. I, II, III, IV denotes different regions.	182
5.8.13	Variation of σ_{AC} with $1000/T$ for the selected LSBMT samples at different frequencies.	183



LIST OF ABBREVIATIONS

LSBMT	$\text{La}_{0.67}(\text{Sr}_{1-x}\text{Ba}_x)_{0.33}\text{Mn}_{1-y}\text{Ti}_y\text{O}_3$
x	Ba composition
y	Ti composition
LCMO	$\text{La}_{1-x}\text{Ca}_x\text{MnO}_3$
LSMO	$\text{La}_{1-x}\text{Sr}_x\text{MnO}_3$
LBMO	$\text{La}_{1-x}\text{Ba}_x\text{MnO}_3$
MR	magnetoresistance
CMR	colossal magnetoresistance
SSR	solid state reaction
FM	ferromagnetic
FMM	ferromagnetic metallic
FMI	ferromagnetic insulator
AF	antiferromagnetic
AFI	antiferromagnetic insulator
PM	paramagnetic
PMI	paramagnetic insulator
CI	canted insulating
SE	superexchange
DE	double exchange
JT	Jahn-Teller
T	temperature
T_C	Curie temperature
T_P	metal-insulator transition temperature



M	magnetization
H	magnetic field
H_C	coercive field
Q_1, Q_2, Q_3	modes of distortion
ρ	resistivity
NNH	nearest neighbour hopping
TAC	thermally activated conduction
SPH	small polaron hopping
VRH	variable range hopping
E_a	energy gap/activation energy
E_p	polaron activation energy
k_B	Boltzmann constant
f	frequency
ω	angular frequency
ω_{max}	maximum angular frequency
R_H	resistance in the presence of a magnetic field
R_0	resistance in the absence of a magnetic field
R_b	bulk/grain resistance
R_{gb}	grain boundary resistance
R_e	interface/electrode resistance
R_T	total resistance
LFMR	low field magnetoresistance
HFMR	high field magnetoresistance
Z^*	complex impedance
Z'	real impedance



Z''	imaginary impedance
ϵ_0	permittivity of free space = 8.854×10^{-12} F/m,
ϵ^*	complex permittivity
ϵ_r	relative permittivity
ϵ'	real part of relative permittivity
ϵ''	imaginary part of relative permittivity
$\tan \delta$	loss tangent/dielectric loss/dissipation factor
Y^*	complex admittance
Y'	real part of complex admittance
Y''	imaginary part of complex admittance
M^*	complex electric modulus
M'	real part of electric modulus
M''	imaginary part of electric modulus
G	conductance
B	susceptance
τ	relaxation time
τ_0	pre-exponential factor
DC	direct current
AC	alternating current
σ_{DC}	direct current conductivity
σ_{AC}	alternating current conductivity
C_0	vacuum capacitance
$C^*, C_n(\omega)$	complex capacitance
C'	real part of capacitance



C''	imaginary part of capacitance
A	cross sectional area of the flat surface
d	thickness of pellet
χ'	real part of susceptibility
χ''	imaginary part of susceptibility
XRD	x-ray diffractometer
SEM	scanning electron microscope
EDX	energy dispersive x-ray
VSM	vibrating sample magnetometer



CHAPTER 1

INTRODUCTION

Perovskite manganite, $\text{Ln}_{1-x}\text{A}_x\text{MnO}_3$ where Ln is an element from the lanthanide group such as La, Nd, Pr, Y and A is a divalent ion such as Ca, Sr, Ba, Pb, with a $\text{Mn}^{3+}/\text{Mn}^{4+}$ mixed valence has stimulated an increasing interest due to their unique spin-dependent magneto-transport properties. A variety of phases such as ferromagnetic metallic (FMM), antiferromagnetic insulator (AFI), ferromagnetic insulator (FMI), cluster glass and spin glass emerged due to the unique coupling among charge, spin, orbital and lattice degree of freedom of the 3d electrons in this system. From the technological point of view, the most intriguing phenomena of this manganese system is the colossal magnetoresistance (CMR) that exists near the Curie temperature, T_C where it experiences a transition from the ferromagnetic (FM) to paramagnetic (PM) state. Extensive research, experimentally and theoretically, on the properties of this material are being done by researchers worldwide (Zener, 1951; Asamitsu et al., 1996; Tokura, 2000; Ziese, 2002; Tokura, 2007) for better understanding of the principles lying behind all those phenomena and hoping that its improved feature could be useful in the technological industries.

The magnetic exchange, structure properties and electronic transport of manganites crucially depend on the $\text{Mn}^{3+}/\text{Mn}^{4+}$ ratio and the effective ionic radius of the A-site cations. These properties are believed to be determined by a competition between the superexchange (SE) and the double exchange (DE) mechanism (Zener, 1951). Further studies of these materials have shown that other mechanism also influences

